

Received October 9, 2019; reviewed; accepted March 30, 2020

Mechanism of micro/nano-bubble formation and cavitation effect on bubbles size distribution in flotation

Xiaowei Deng ^{1,2}, Bo Lv ¹, Gan Cheng ¹, Yang Lu ¹¹ College of Chemistry and Chemical Engineering, Henan Polytechnic University, Jiaozuo 454000, China² Coal Production Safety Collaborative Innovation Center in Henan Province, Henan Polytechnic University, Jiaozuo 454000, China

Corresponding author: lvbo2158@126.com (Bo Lv)

Abstract: In this study, micro/nano-bubble generated by cavitation effect as a promoting factor for flotation was investigated using the atomic force microscope (AFM). Hydrodynamic cavitation tests were performed with a venturi bubble generator. Additionally, bubble size distribution (BSD) under the hydrodynamic cavitation effect was also studied at different water flow speed conditions. Dozens of nanometers height bubbles attached to the hydrophobic substrates were detected. Besides, the cavitation cloud grew thicker with the flow velocity increasing from 26.52 m/sec to 53.04 m/sec, near the venturi tube nozzle. All results showed the importance of the cavitation effect on the micro/nano-bubbles formation and the BSD in flotation.

Keywords: micro/nano-bubbles, cavitation effect, bubble size distribution, flotation

1. Introduction

Micro/nano-bubbles formation mechanism, depend on dynamics and thermodynamics process of the fluid environment, is an important factor for improving understanding of the flotation bubble characteristics (Zhou et al., 2008; Emin et al., 2015; Li et al., 2016). In this process, the cavitation included hydrodynamic cavitation and supersaturated cavitation is the critical factor for micro/nano-bubbles formation. It is well known that the cavitation is defined as a function not only of the saturation vapor pressure decreased in flotation but also of plenty of cavitation nuclei in water (Yount, 1997; Liu, 2017). It is presented as:

$$P_1 + \frac{1}{2} \rho_w u_{w1}^2 = P_2 + \frac{1}{2} \rho_w u_{w2}^2 = C \quad (1)$$

where u_{w1} and u_{w2} are flow velocities at different points in the same flow system respectively, P_1 and P_2 are pressures at different points respectively, ρ_w is water density, C is a constant.

The cavitation effect is not well understood since it is influenced by the aeration and the mineral particle characteristics in flotation. In the case without aeration, high speed rotating impeller within the flotation machine could produce a lot of cavities, but the cavitation bubbles would collapse with the flow velocity or the pressure decreasing. Eq. 2 (Teixeira et al., 2006) presents the relationship between the impeller surface pressure P_{im} and impeller rotate speed N_r in water.

$$P_{im} = P_0 + \rho_w gh - \frac{1}{2} \rho_w N_r^2 C_b \quad (2)$$

where P_0 is the local atmospheric pressure, h is the impeller depth submerged in water, and C_b is the coefficient related to the impeller.

Supersaturated cavitation is the main way of micro/nano-bubble formation in the low-pressure zone of the dissolution air flotation machine with the saturation vapor pressure decreasing (Zhou et al., 1996). There are also a wide range of low-pressure zone in the jet flow machine and the machinery stirring

flotation machine. In such a case, tiny bubbles (nanometer and micrometer level) can generate on a solid surface (Henderson et al., 2008a, 2008b, 2008c). It is hard to come out cavitation in pure water because there are not enough cavitation nuclei. The good news is that mineral particles and gas nuclei provide sufficient cavitation nuclei in the flotation system (Lurie and Rebhun, 1997; Zhou et al., 1998; Zhou et al., 1999; Fan et al., 2010a; Verrelli et al., 2011). Abundant tiny bubbles ($< 100 \mu\text{m}$) by cavitation are beneficial to float fine minerals and aggregates, particularly in the low-pressure zone. This level of pressure is two orders of magnitude lower than the supersaturation required for spontaneous nucleation of bubbles in bulk water (Yount and Kunkle, 1975; Oliveira and Rubio, 2011). It implies that cavitation bubbles formation needs to have both pressure decrease and process initiation.

In the agitation and jet process of flotation, the aeration provides a source of bubbles, meanwhile, the cavitation plays a key role in the tiny bubble formation. In this study, the main aim was to illuminate the cavitation effect which promotes micro/nano-bubbles formation and influences bubbles size.

2. Experimental

2.1. Materials and methods

Several methods such as bubble size distribution (*BSD*) and bubble surface area flux (*BSAF*) can be used to determine the bubble characteristics and the influence factors of flotation (Nguyen et al., 2006; Assemi et al., 2008). In this study, some experiments were carried out by using a series of substrates (diameter 10mm), analytical anhydrous ethanol, enough ultrapure water (after multi-stage filtration, high-performance ion exchange, ultrafiltration filter, ultraviolet ray removal processing, the resistivity $> 18 \text{ m}\Omega\cdot\text{cm}$), two syringe pumps (10 cm^3), a special glass venturi tube bubble generator and a set of flotation machine impeller device.

The hydrophobicity of Au and Pb materials surfaces can fit the bubbles generation requirements. In the experiment, the Au and Pb substrates, surface relief $< 5 \text{ nm}$ measured by *AFM*, were used in the micro/nano-bubble sample preparation and the micro/nanobubbles characteristic testing. Each substrate was fixed on the sample vessel bottom by three buckles equably. To analyze the effect of nano-bubble on the Au and Pb substrates surface, the contact angle was measured by a *DSA100* measurement instrument (contact angle measurement range: $0\sim 180^\circ$, resolution: $\pm 0.01^\circ$) before micro/nano-bubble preparation. The contact angles of Pb and Au substrates were measured as 26° and 75° , respectively, as seen in Fig. 1.

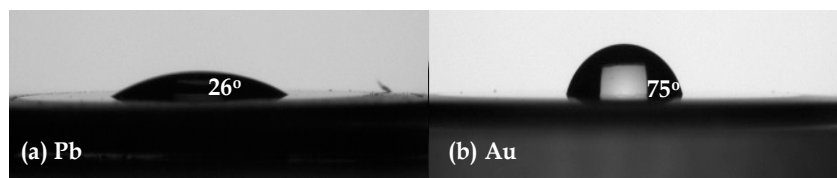


Fig. 1. Contact angle of (a) Pb and (b) Au substrates

The special glass venturi tube was used to investigate the cavitation effect. A schematic diagram is shown in Fig. 2. The feeding pipe diameter (d_1) is 11mm, and the nozzle diameter (d_2) is 1.5 mm. This kind of the venturi bubble generators was widely used in various flotation equipment such as Jameson flotation column (Jameson et al., 2007), jet flotation machine (Chanson et al., 2004), cyclonic micro-bubble flotation column, etc. (Zhang et al., 2009; Cao et al., 2009). With flow speed increasing in the nozzle, negative pressure initiates and then causes aeration near the gas-liquid interface in the gas cham-

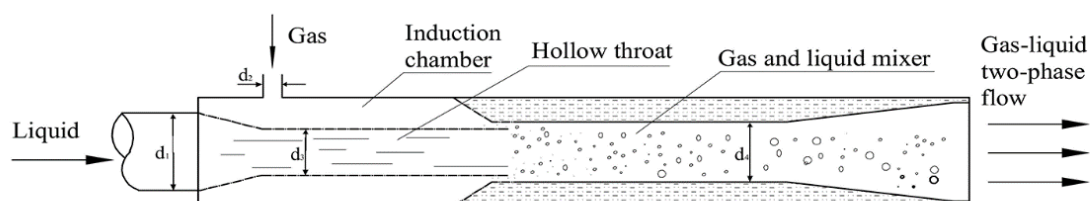


Fig. 2. Special glass venturi tube

ber (or aeration room) (Bhattacharjee et al., 1998; Miller et al., 1999; Paunov et al., 2002; Tao, 2004; Dressaire et al., 2008). The consecutive aeration results in a powerful suction effect. Air volume can be controlled through an inlet valve yet.

2.2. Supersaturated cavitation tests

There are quite a few literature reported using the tap mode of *AFM* for the micro/nano-bubbles measurement (Assemi et al., 2006a; Assemi et al., 2006b; Hampton and Nguyen, 2010). The intelligent mode of a German Bruker *AFM* was adopted in this experiment. For the intelligent mode, surface bubbles destruction and slip are smaller than the tap mode, in the needle scanning process.

The sample vessels with the substrates were cleaned by 15% sodium pyruvate solution and then were put into the ultrasonic cleaning machine for 30 min cleaning. Finally, the surface of the substrate was washed 2~3 times with ultrapure water again and was dried by nitrogen gas. Next, 99.9% ethanol was injected in the Au and Pb sample vessels respectively, until each substrate was just submerged. Subsequently, ultrapure water was poured into both of the sample vessels respectively, at the same time the half of the alcohol-water mixture in the sample vessel was sucked out by a syringe pump quickly. At the moment, micro/nano-bubbles would generate on the surface of the substrate, because the saturated vapor pressure of ethanol is greater than pure water at the same temperature and pressure conditions. When alcohol was replaced by pure water, dissolved air was coagulated on the substrate surface to form micro/nanobubbles further (Azevedo et al., 2016). Certainly, when environment pressure reduces, the saturated vapor pressure of the same liquid would decrease and then generate micro/nano-bubbles yet at the same temperature. Micro/nano-bubbles formed by the alcohol and water displacement on substrates surface were scanned through the intelligent model of Bruker *AFM* in $5\ \mu\text{m} \times 5\ \mu\text{m}$ range.

2.3. Hydrodynamic cavitation tests

Negative pressure also produces in the back zone of the impeller rotor and the venturi tube nozzle in flotation devices (Xu et al., 1996; Filippov et al., 2000). Compared to the impeller rotor, there is a higher flow speed in the venturi nozzle. The process of jet cavitation at the venturi tube nozzle was investigated by using a high-speed dynamic camera at 1500 fps. In the experiment, the inlet valve of the venturi tube was closed. When flow volumes of the peristaltic pump were $300\ \text{dm}^3/\text{h}$, $400\ \text{dm}^3/\text{h}$, $500\ \text{dm}^3/\text{h}$, and $600\ \text{dm}^3/\text{h}$ separately and nozzle diameter was 2 mm, the velocities of jet flow were 26.52 m/sec, 35.36 m/sec, 44.20 m/sec, and 53.04 m/sec separately at the nozzle. The cavitation phenomenon could be observed at different flow velocities.

2.4. Tests of cavitation effect on BSD

To study the cavitation effect on *BSD*, the bubbles attached to the Pb and Au substrates were measured by a Carl Zeiss polarizing microscope. At first, the venturi tube bubble generator and the bubbles sample vessel with different substrates were cleaned 30 min by an ultrasonic cleaning machine and then were flushed with ultrapure water 2~3 times again. Air volumes were adjusted by the inlet valve and the bubbles sample vessel was put in the $3\ \text{dm}^3$ water cell. When the flow velocities in the nozzle of the bubble generator at 26.52 m/sec and 35.36 m/sec severally, 10 min later, the bubbles sample vessel filled with water was taken out from the cell using a tweezers cautiously. Then, the substrate's surface attached with a lot of bubbles in the sample vessel was observed by a microscope ($\times 10$ oil lens and $\times 10$ lens) with ProgRes C5 image capture and processing system. A series of bubble images were imported into the Image-Pro Plus 7.0c software. *BSD* data of different hydrophobic substrates surface could be got using the method of gray shadow.

3. Results and discussion

3.1. Supersaturated cavitation effect

Fig. 3 presents the measurement result of micro/nano-bubbles precipitated on the Pb substrate by *AFM*. Fig. 3(a) shows the solid surface morphology of the Pb substrate before alcohol-water displacement. The

scanning range was $5\ \mu\text{m} \times 5\ \mu\text{m}$, and the surface undulation height was 6.1 nm (measurement accuracy was 1 nm). The Pb substrate surface is flat and regular from the result. Besides, Fig. 3(b) shows the Pb substrate surface after alcohol-water displacement. As well, the scanning range was $5\ \mu\text{m} \times 5\ \mu\text{m}$, and the surface undulation height was 6.3 nm. However, a mass of nano-bubbles, a diameter of about 100 nm and a height of about 20 nm on the Pb substrate can be distinguished clearly. Since there were not any contaminations in the experimental process, the supersaturated cavitation effect generated the nano-bubbles.

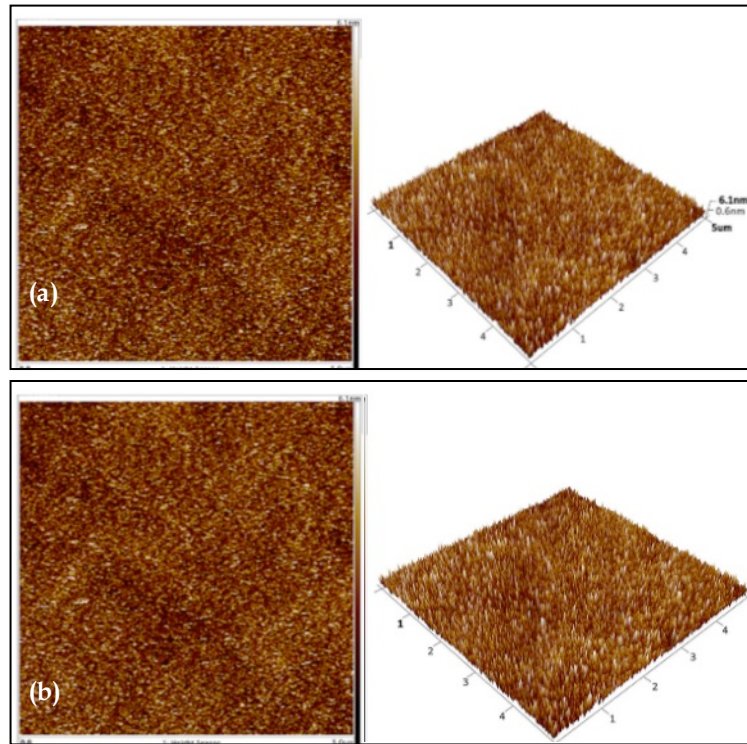


Fig. 3. AFM results of (a) solid configuration and (b) micro/nano-bubbles precipitated on Pb substrates

Fig. 4 presents the measurement result of micro/nano-bubbles precipitated on the Au substrate by AFM. Figure 4(a) shows a solid surface configuration of the Au substrate before alcohol-water displacement. The scanning range was $5\ \mu\text{m} \times 5\ \mu\text{m}$. Au substrate inclining height was 43 nm, and the surface undulation height was 4 nm (measurement accuracy was 1 nm). Figure 4(b) shows the Au substrate surface after the alcohol-water displacement. As well, the scanning range was $5\ \mu\text{m} \times 5\ \mu\text{m}$, and the surface undulation height was 3 nm. Plenty of bright spots distributed on the Au substrate surface can be distinguished clearly. The big bright spot diameter was about 300 nm, and the height was about 40nm. Similarly, the bright spots were identified as micro/nano-bubbles after contrasting and analyzing the Au substrates in different conditions.

As seen in Figs. 3 and 4, there are more micro/nano-bubbles on the Au substrate surface compare with Pb substrate surface, because the hydrophobicity of Au is greater than Pb. The micro/nano-bubbles attached to the mineral surface can provide a significant enhancement in the collision and adhesion process of air bubbles and mineral particles (Schubert, 2005; Ahmed, 2010). It is known that micro/nano-bubbles attach to particle surface more stable than conventional bubbles (Fan et al., 2010b; Fan et al., 2010c; Ushikubo et al., 2010; Hang and Massoud, 2014.). In such a case, micro/nano-bubbles increase fine mineral hydrophobicity. The experimental results showed that supersaturated cavitation can generate nano-bubble cluster on a solid surface, and then promote bubble mineralization in flotation.

3.2. Hydrodynamic cavitation effect

As all known, flow velocity plays a key role in hydrodynamic cavitation. Under the same temperature and pressure condition, when one kind of liquid with high saturated vapor pressure is displaced by

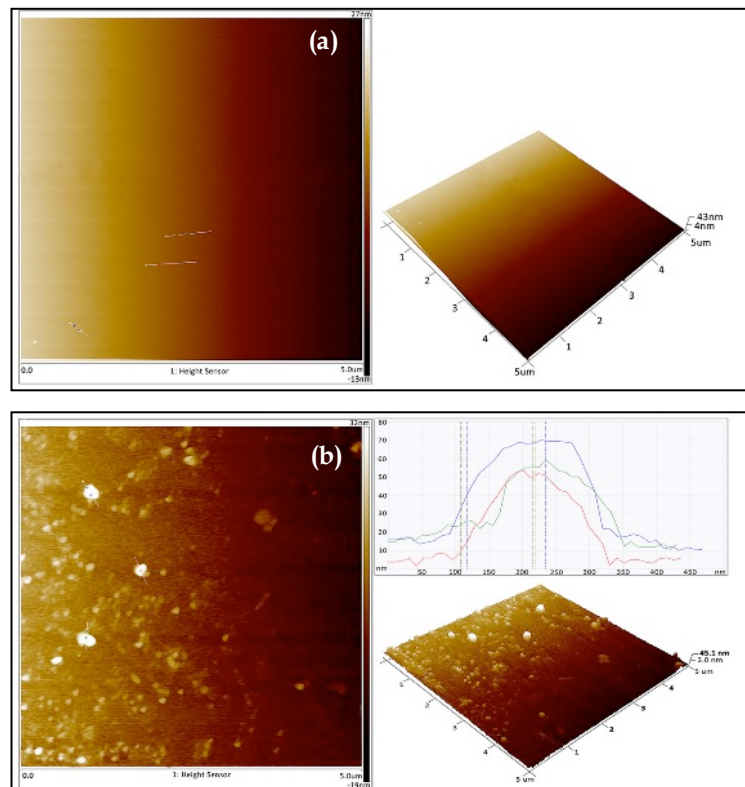


Fig. 4. AFM results of (a) solid configuration and (b) micro/nano-bubbles precipitated on Au substrates

another low saturated vapor pressure liquid, the supersaturation cavitation generates micro/nano-bubbles on the hydrophobic solid surface. Similarly, for the same kind of liquid at the same temperature, the environment pressure drops can also cause supersaturated cavitation, and then produce micro/nano-bubbles.

Fig. 5 shows hydrodynamic cavitation results at different flow velocity of gradual change in the nozzle of the venturi tube. When the water flow passes through the nozzle, flow rate and pressure gradually reduce with the pipe diameter increasing. Both of the pressure increases and fluid shear cause an obvious cavitation cloud near the nozzle (Dong and Su, 2006). When the flow velocity increases from 26.52 m/sec to 53.04 m/sec, the cavitation cloud intensity strengthens gradually. The viscous force and the drag force leading to flow velocity decrease, which caused by shearing action between the fluid micelle. Therefore, the cavities belong to vortex cavitation, and the low-pressure area in the vortex center can generate cavitation nuclei.

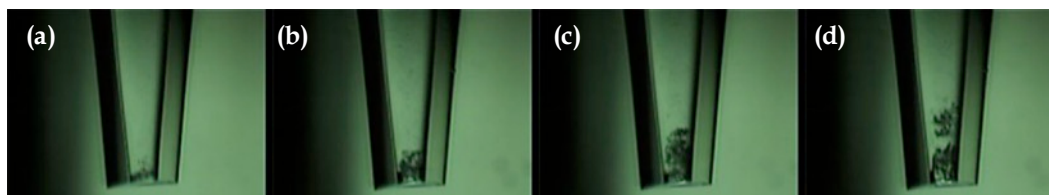


Fig. 5. Results for hydrodynamic cavitation at different flow velocity of gradual change in the nozzle of the venturi tube (a) 26.53 m/sec (b) 35.36 m/sec (c) 44.20 m/sec (d) 53.04 m/sec

Fig. 6 shows hydrodynamic cavitation results at different flow velocity of gradual change near the nozzle of the venturi tube. With flow velocity decreasing suddenly, the cavitation cloud appears more obvious. When the flow velocity increases from 26.52 m/sec to 53.04 m/sec, the cavitation cloud intensity strengthens suddenly. Compare with the gradual change of flow velocity, the cavitation cloud intensity and scope at sudden change conditions are greater, due to greater pressure drop and fluid shear stress. As previously mentioned, this hydrodynamic cavitation can produce a large number of

micro/nano-bubbles, these contribute to the flotation of fine-grained minerals (Bhondayi and Moys, 2014). In that case, stronger hydrodynamic cavitation will have a greater impact on flotation bubbles.

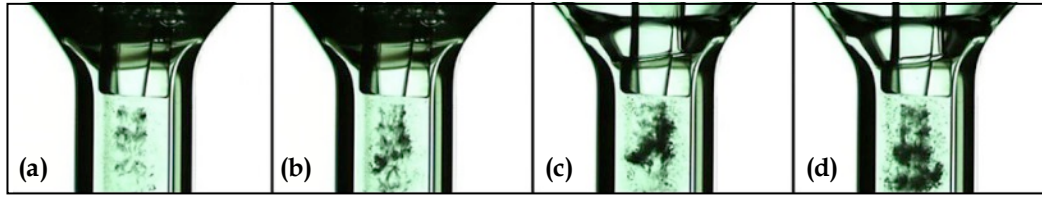


Fig. 6. Cavitation results at different flow velocity of leap change near the nozzle of the venturi tube (a) 26.53 m/sec (b) 35.36 m/sec (c) 44.20 m/sec (d) 53.04 m/sec

3.3. Cavitation effect on BSD

As previously described, hydrodynamic cavitation can affect bubble size in flotation, however flow velocity plays a key role in hydrodynamic cavitation. The *BSD* under the cavitation effect at 26.52 m/sec and 35.36 m/sec flow velocity was given in Figs. 7 and 8, respectively. The venturi tube bubble generator was used to generate bubbles with sudden change flow velocity. The *BSD* determined from the measurement was performed with Au and Pb substrates. For each experiment condition, 50 photos collected from the different zone of each substrate identified by gray differences were statistically analyzed, respectively. Both for Pb and Au, the biggest bubble diameter D_{max} is 600 μm , however, the D_{min} is 10 μm . On the Au substrate surface, the bubbles were more than the Pb substrate at different nozzle flow velocity. Compare with 26.52 m/sec flow velocity, the bubble quantities with 35.36 m/sec were greater. From the results of *BSD*, the biggest proportion of bubbles was distributed at 10~50 μm range.

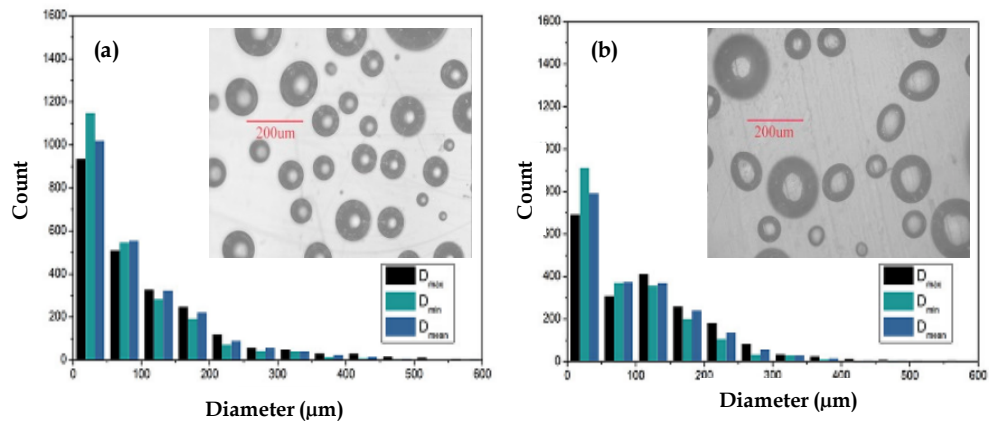


Fig. 7. *BSD* on (a) Au and (b) Pb surface at 26.52 m/sec flow velocity

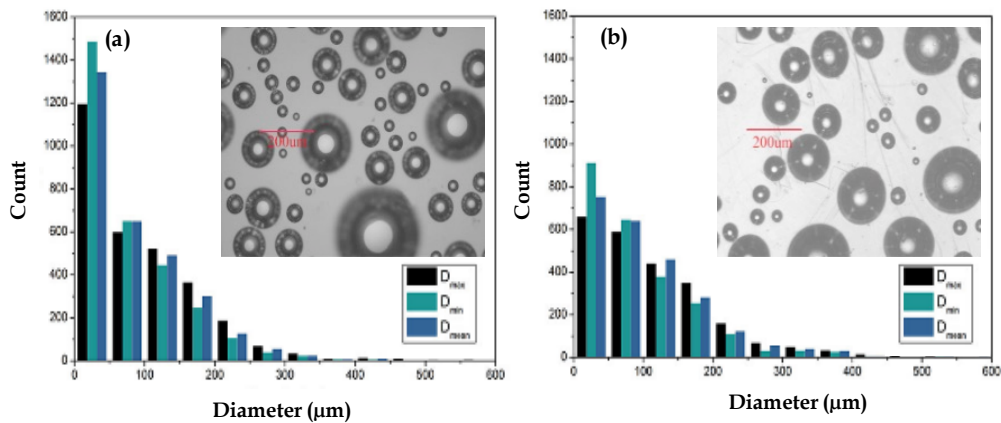


Fig. 8. *BSD* on Au and Pb surface at 35.36 m/sec flow velocity

As seen in Figs. 7 and 8, the plentiful of $-50\ \mu\text{m}$ tiny bubbles attach on the Au surface, and the greater flow velocity is, the more bubbles attached on the substrate surface. It illustrates that the cavitation effect plays a significant influence on the bubble's size. As all know, enormous energy generated by hydrodynamic cavitation bubbles collapse could etch the structure of equipment in flotation. However, on Au and Pb surface, when flow velocity increase from 26.52 m/sec to 35.36 m/sec, bubble size decrease gradually, but the bubble number increase. It might be related to the collapse of energy generated by the hydrodynamic cavitation impact on the air bubble surface. The enormous collapse energy of cavitation can laminate the air bubble and split it into tiny bubbles. As previously mentioned, the pressure drop which leads to nano-bubble production is accompanied by the hydrodynamic cavitation generation. In flotation, the cavitation effect on *BSD* appears in two aspects. The first is the nano-bubble production by pressure drop and the second is the tiny bubble generation by cavitation bubbles collapsing on air bubbles. Therefore, the hydrodynamic cavitation effect can prompt tiny bubbles and gas nuclei the formation which is conducive to fine mineral particle recovery in flotation.

4. Conclusions

In this study, micro/nano-bubble generated by the cavitation effect as a promoting factor for flotation was investigated by the AFM. Hydrodynamic cavitation tests were performed with a venturi bubble generator. Additionally, the *BSD* under the hydrodynamic cavitation effect was also studied at different water flow speed conditions. Dozens of nanometers height bubbles attached to the hydrophobic substrates were detected. The following results were obtained from this study:

Air is always surplus in the flotation process due to aeration. On the one hand, a lot of micro/nano-bubbles attach to the hydrophobic particles generated by supersaturated cavitation, on the other hand, plenty of tiny bubbles are formed by hydrodynamic cavitation. A part of micro/nano-bubbles and tiny bubbles could dissolve in water in the high-pressure zone, but dissolved air could coagulate to gas micronucleus in the low-pressure zone yet.

The results of supersaturated cavitation and surface nano-bubbles tests indicate that a few hundred nanometers width and 10-40 nm height bubbles formed on the different hydrophobicity surface. Besides, the more hydrophobicity of the surface is, the more micro/nano-bubbles generate and attach on the surface.

The hydrodynamic cavitation cloud was detected obviously near the venturi tube nozzle at the different flow velocity conditions. Flow velocity and pressure drop determine the hydrodynamic cavitation intensity and tiny bubbles quantity.

It can be concluded from this study that the hydrodynamic cavitation effect promotes the tiny bubble proportion in bubble size distribution. Tiny bubbles are conducive to fine and slow-floating mineral particle flotation.

Acknowledgments

The authors gratefully acknowledge the National Natural Science Foundation of China (51904096). Science and Technology Project of Henan Province (172102310641)

References

- AZEVEDO, A., ETCHEPARE, R., CALGAROTO, S., 2016. *Aqueous dispersions of nano bubbles: Generation, properties and features*. Minerals Engineering, 94(8), 29-37.
- ASSEMI, S., NALASKOWSKI, J., JOHNSON, W.P., 2006a. *Direct force measurements between carboxylate-modified latex microspheres and glass using atomic force microscopy*. Colloids and Surfaces A: Physicochemical and Engineering Aspects, 286, 70-77.
- ASSEMI, S., NALASKOWSKI, J., JOHNSON, W.P., 2006b. *Isoelectric point of fluorite by direct force measurements using atomic force microscopy*. Langmuir, 22(4), 1403-1405.
- ASSEMI, S., NGUYEN, A.V., MILLER, J.D., 2008. *Direct measurement of particle-bubble interaction forces using atomic force microscopy*. International Journal of Mineral Processing, 89, 65-70.
- AHMED, M.M., 2010. *Effect of comminution on particle shape and surface roughness and their relation to flotation process*. Int. J. Miner. Process., 94(3), 180-191.

- BHONDAYI, C., MOYS, M.H., 2014. *Measurement of a proxy for froth phase bubble sizes as a function of froth depth in flotation machines Part 1. Theoretical development and testing of a new technique.* International Journal of Mineral Processing, 130(7), 8-19.
- BHATTACHARJEE, S., KO, C.H., ELIMELECH, M., 1998. *DLVO interaction between rough surfaces.* Langmuir, 14(12), 3365-3375.
- CHANSON, H., AOKI, S., HOQUE, A., 2004. *Physical modeling and similitude of air bubble entrainment at vertical circular plunging jets.* Chemical Engineering Science, 59, 747-758.
- CAO, Y.J., GUI, X.H., MA Z.L., 2009. *Process mineralogy of copper-nickel sulphide flotation by a cyclonic-static micro-bubble flotation column.* Mining Science and Technology, 19, 0784-0787.
- DONG, Z.Y., SU, P.L., 2006. *Cavitation control by aeration and its compressible characteristics.* Journal of Hydrodynamics, 18(4), 99-504.
- DRESSAIRE, E., BEE, R., BELL, D., LIPS, A., STONE, H., 2008. *Interfacial polygonal nano patterning of stable microbubbles.* Science, 320, 1198-1201.
- EMIN, C.C., SEVGI, K., 2015. *Effect of nanoparticles on froth stability and bubble size distribution in flotation.* International Journal of Mineral Processing, 138, 6-14.
- FAN, M., TAO, D., HONAKER, R., LUO, Z., 2010a. *Micro/nano-nano bubble generation and its application in froth flotation (Part I): Micro/nano-nano bubble generation and its effects on the properties of microbubble and millimeter scale bubble solutions.* Mining Science Technology, 20(1), 1-19.
- FAN, M., TAO, D., HONAKER, R., LUO, Z., 2010b. *Micro/nano-nano bubble generation and its application in froth flotation (Part II): Fundamental study and theoretical analysis.* Mining Science Technology, 20(2), 159-177.
- FAN, M., TAO, D., HONAKER, R., LUO Z., 2010c. *Micro/nano-nano bubble generation and its application in froth flotation (Part III): Specially designed laboratory scale column flotation of phosphate.* Mining Science Technology, 20(3), 317-338.
- FILIPPOV, L.O., JOUSSEMET, R., HOUOT, R., 2000. *Bubble spargers in column flotation adaptation to precipitate flotation.* Minerals Engineering, 13(1), 37-51.
- HENDERSON, R.K., BAKER, A., PARSONS, S.A., JEFFERSON, B., 2008a. *Characterization of algogenic organic matter extracted from cyanobacteria green algae and diatoms.* Water Research, 42(13), 3435-3445.
- HENDERSON, R.K., PARSONS, S.A., JEFFERSON, B., 2008b. *Successful removal of algae through the control of zeta potential.* Separation Science Technology, 43(7), 1653-1666.
- HENDERSON, R.K., PARSONS, S.A., JEFFERSON, B., 2008c. *Surfactants as bubble surface modifiers in the flotation of algae: dissolved air flotation that utilizes a chemically modified bubble surface.* Environmental Science and Technology, 42(13), 4883-4888.
- HANG, J.J., MASSOUD, K., 2014. *Heterogeneous bubble nucleation on ideally-smooth horizontal heated surface.* International Journal of Heat and Mass Transfer, 71, 149-157.
- HAMPTON, M.A., NGUYEN, A.V., 2010. *Micro/nanobubbles and the micro/nano-nanobubble bridging capillary force.* Advances in Colloid Interface Science, 154, 30-55.
- JAMESON, G.J., NGUYEN, A.V., ATA, S., 2007. *The flotation of fine and coarse particles.* Froth Flotation a Century of Innovation. SME, pp. 339-372.
- LI, X.B., XU, H.X., LIU, J.T., ZHANG, J., GUIZ, L., 2016. *Cyclonic state micro-bubble flotation column in oil-in-water emulsion separation.* Separation and Purification Technology, 165(13), 101-106.
- LURIE, M., REBHUN, M., 1997. *Effect of properties of polyelectrolytes on their interaction with particulates and soluble organics.* Water Science Technology, 36, 93-101.
- LIU, L.T., YAO, X.L., LIU, N.N., YU, F.L., 2017. *Toroidal bubble dynamics near a solid wall at different Reynolds number.* International Journal of Multiphase Flow, 13(9), 211-220.
- MILLER, J.D., HU, Y., VEERAMASUNENI, S., LU, Y., 1999. *In-situ detection of butane gas at hydrophobic silicon surfaces.* Colloids and Surfaces, 154, 137-147.
- NGUYEN, A.V., PHAN, C.M., EVANS, G.M., 2006. *Effect of the bubble size on the dynamic adsorption of frothers and collectors in flotation.* International Journal of Mineral Processing, 79, 18-26.
- OLIVEIRA, C., RUBIO, J., 2011. *Zeta potential of single and polymer-coated microbubbles using an adapted micro electrophoresis technique.* International Journal of Mineral Processing, 98(12), 118-123.
- PAUNOV, V.N., BINKS, B.P., ASHBY, N.P., 2002. *Adsorption of charged colloid particles to charged liquid surfaces.* Langmuir, 18, 6946-6955.

- SCHUBERT, H., 2005. *Micro/nanobubbles, hydrophobic effect, heterocoagulation and hydrodynamics in flotation*. International Journal of Mineral Processing, 78, 11-21.
- TEIXEIRA, M.R., ROSA, M.J., 2006. *Comparing dissolved air flotation and conventional sedimentation to remove cyanobacterial cells of Microcystis aeruginosa: Part I: The key operating conditions*. Separation Purification Technology, 52(1), 84-94.
- TAO, D., 2004. *Role of bubble size in flotation of coarse and fine particles-a review*. Separation Science Technology, 4(39), 741-760.
- USHIKUBO, F.Y., FURUKAWA, T., NAKAGAWA, R., ENARI, M., MAKINO, Y., KAWAGOE, Y., 2010. *Evidence of the existence and the stability of nano-bubbles in water*. Colloids and Surfaces A: Physicochemical and Engineering Aspects, 361, 31-37.
- VERRELLI, D. I., KOH, P.T.L., NGUYEN, A.V., 2011. *Particle-bubble interaction and attachment in flotation*. Chemical Engineering Science, 66(23), 5910-5921.
- XU, M., QUINN, P., STRALLON-CRAWLY, R., 1996. *A feed-line aerated flotation column. Part 1: Batch and continuous test work*. Mining Engineering, 9(5), 499-508.
- YOUNT, D.E., 1997. *On the elastic properties of the interfaces that stabilize gas cavitation nuclei*. Colloid Interface Science, 193, 50-59.
- YOUNT, D.E., KUNKLE, T.D., 1975. *Gas nucleation in the vicinity of solid hydrophobic spheres*. Journal of Applied Physics, 46(10), 4484-4486.
- ZHOU, Z.A., CHOW, R., XU Z.H., MASLIYAH, J.M., ZHOU, Z.A., CHOW, R., XU Z.H., MASLIYAH, J.M., 2008. *Spontaneous bubble nucleation on bitumen*. In: XXIV International Mineral Processing Congress, Beijing, China, 24-28.
- ZHOU, Z.A., XU, Z.H., FINCH, J.A., 1996. *Effect of gas nuclei on hydrophobic coagulation*. Journal of Colloid and Interface Science, 179, 311-314.
- ZHOU, Z.A., XU, Z.H., FINCH, J.A., 1998. *Effect of surface properties of solids on dynamic bubble formation in gas-supersaturated systems*. Industrial & Engineering Chemistry Research, 37,1998-2004.
- ZHOU, Z.A., XU, Z.H., FINCH, J.A., 1999. *Generation of small bubbles by hydro dynamic cavitation*. Trans. IMM., 108, 55-58.
- ZHANG, M., SHI, C.S., LIU, J.T., ZHAI, A.F., 2009. *A honeycomb-tube packing medium and its application to column flotation*. Mining Science and Technology, 19, 775-778.